A Numerical Study on the Compressibility of Subblocks of Schur Complement Matrices Obtained from Discretized Helmholtz Equations

Martin J. Gander[1] and Sergey Solovyev[2]

[1] Section of Mathematics, University of Geneva, Switzerland,
martin.gander@unige.ch,
[2] Institute of Petroleum Geology and Geophysics SB RAS,
3 Akademika Koptyuga pr., Novosibirsk, Russia, 630090
solovevsa@ipgg.sbras.ru

Abstract. The compressibility of Schur complement matrices is the essential ingredient for $\mathcal{H}$-matrix techniques, and is well understood for Laplace type problems. The Helmholtz case is more difficult: there are several theoretical results which indicate when good compression is possible with additional techniques, and in practice sometimes basic $\mathcal{H}$-matrix techniques work well. We investigate the compressibility here with extensive numerical experiments based on the SVD. We find that with growing wave number k, the ϵ-rank of blocks corresponding to a fixed size in physical space of the Green's function is always growing like $O(k^\alpha)$, with $\alpha \in [\frac{3}{4}, 1]$ in 2d and $\alpha \in [\frac{4}{3}, 2]$ in 3d.

Keywords: Helmholtz Equation, Schur Complements, ϵ-Rank

1 Introduction

After their introduction in the seminal paper by Hackbusch [23], $\mathcal{H}$-matrix techniques have been intensively developed over the last two decades to represent dense matrices arising from discretizations of integral equations as well as perform operations between such matrices with almost linear complexity; for a comprehensive introduction including most recent results, see [3, 24]. These techniques are very much related to the fast multipole method introduced by Greengard and Rokhlin [22], which also uses the fact that the Green's functions of Laplace like problems have favorable properties; for a recent overview, see [21], and for sharp estimates for $\mathcal{H}$-matrices approximating inverses of FEM-discretized Laplace like operators, see [4].

The fast multipole method has also been studied for wave propagation phenomena [27, 8], of which a typical representative is the Helmholtz equation. Although the Helmholtz equation has the deceivingly simple looking Laplacian as its principal part, the difficulty of its numerical solution is worlds apart from solving Laplace's equation; for a recent overview why standard iterative methods fail in the Helmholtz case, see [14]. Specialized methods were developed

for the Helmholtz equation: AILU methods based on analytic incomplete LU factorizations [18, 19], reinvented independently later under the name sweeping preconditioner [11, 12], and optimized Schwarz methods (OSM) [17, 16], which represent a unified framework for all these methods, see [20]. For an introduction to OSM, see [15].

To use $\mathcal{H}$-matrix techniques for the Helmholtz equation proves also to be more difficult: in [2], the subblocks arising are partitioned into two different types, one of which can be well treated by $\mathcal{H}^2$-matrix techniques, whereas for the other one, a multipole like expansion is needed. Almost linear complexity for the compression with a directional $\mathcal{H}^2$-matrix technique is obtained in [6], but there is no complete $\mathcal{H}^2$-matrix arithmetic available yet. For a specific geometric situation, almost linear complexity was also shown in the multipole context in [26]. Upper and lower bounds for the separability of the Green's function of the Helmholtz operator recently derived in [13] indicate however that in general the number of terms is expected to grow algebraically in the wave number. Nevertheless, even the basic $\mathcal{H}$-matrix approach was observed to work quite well in certain situations, see for example [5, 25].

We study here the compressibility of off diagonal blocks of Schur complement matrices for the Helmholtz equation numerically using the SVD. We investigate the dependence of the compressibility on the wave number, mesh size, subblock selection and boundary conditions. While for the Laplace case there is a precise theoretical study for the finite difference discretizations we use [7], both in 2d and 3d, for the Helmholtz equation to the best of our knowledge this remains an open question. We measure that the ϵ-rank grows in all our numerical experiments algebraically in the wave number, and the growth is faster in 3d than in 2d.

2 Two Dimensional Study

We study the Helmholtz equation

$$\begin{array}{rl} (\Delta + k^2)u = f & \text{in } \Omega := (0,1)^2, \\ \mathcal{B}u = 0 & \text{on } \partial\Omega, \end{array} \tag{1}$$

where $\mathcal{B}$ denotes a suitable boundary operator of Dirichlet and Robin type for the problem to be well posed, and we will be testing various configurations. We discretize the Helmholtz equation (1) using a standard five point finite difference discretization with mesh spacing $h := \frac{1}{n}$, which leads to a sparse linear system

$$A\boldsymbol{u} = \boldsymbol{f}. \tag{2}$$

If we partition the system matrix into a first block A_1 corresponding to the first line of discretization points in the y-direction, and denote the remaining diagonal block by A_2, the linear system (2) can be written in the form

$$\begin{pmatrix} A_1 & A_{12} \\ A_{21} & A_2 \end{pmatrix} \begin{pmatrix} \boldsymbol{u}_1 \\ \boldsymbol{u}_2 \end{pmatrix} = \begin{pmatrix} \boldsymbol{f}_1 \\ \boldsymbol{f}_2 \end{pmatrix}. \tag{3}$$

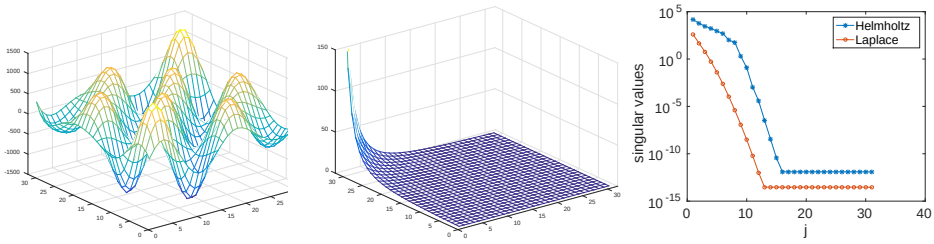

Fig. 1. Real part of the off diagonal block $S_{31,40.2}$ of the Schur complement of the Helmholtz operator (left) and the Laplace operator (middle) for Dirichlet boundary conditions, and their singular values σ_j (right).

Note that the vectors $\boldsymbol{u}_1$ and $\boldsymbol{f}_1$ correspond to only one line of unknowns and are thus much shorter than $\boldsymbol{u}_2$ and $\boldsymbol{f}_2$. We are interested in the Schur complement matrix S of the reduced system indicated by the partition in (3), i.e. when all the unknowns $\boldsymbol{u}_2$ are eliminated from the system,

$$S\boldsymbol{u}_1 = \boldsymbol{f}_1 - A_{12}A_2^{-1}\boldsymbol{f}_2, \quad S := A_1 - A_{12}A_2^{-1}A_{21}. \tag{4}$$

The representation of the Schur complement matrix S as an $\mathcal{H}$-matrix requires to form the so called block cluster tree, which is a partition of S into subblocks, and then to approximate these subblocks by low rank matrices. In the case of Laplace's equation, blocks on the diagonal of S or close to the diagonal can not be compressed well, since they are close to the singularity of the Green's function of Laplace's equation that lies on the diagonal. Blocks far away from the diagonal however can be very well compressed in the Laplace like cases [4]. To study the compressibility in the Helmholtz case, we apply the singular value decomposition (SVD) to the matrix subblock $S_{m,k} := S(1:m, n-m+1:n)$ of the Schur complement matrix $S \in \mathbb{C}^{n\times n}$ and study the decay of the singular values as a function of m, h, and k.

We start by showing in Figure 1 for $n = 64$ on the unit square and $k = 40.2$ the off diagonal block of the Schur complement $S_{m,k}$ of the discretized Helmholtz operator with Dirichlet boundary conditions for $m = 31$ on the left, and for comparison purposes also the corresponding Laplace case with $k = 0$ in the middle. We can clearly see that the fundamental solution visible in the Schur complement is very oscillatory for the Helmholtz operator, while it is much simpler and just decaying for the Laplace operator. This has an important influence on the decay of the singular values σ_j of these blocks, as one can see on the right: the decay in the Helmholtz case is delayed. This influences the ϵ-rank, which is defined as the smallest number r_ϵ such that $\frac{\sigma_j}{\sigma_1} < \epsilon$ for all $j > r_\epsilon$, i.e the number of singular values we have to keep so that the approximate matrix is at most at a distance ϵ from the exact matrix in the Frobenius norm.

We next show in Table 1 the ϵ-rank of the approximate Schur complement $S_{m,k}$ for increasing k when using 10 ppw for the discretization, i.e. $k = \frac{2\pi n}{10}$, where n is the number of mesh cells in one space direction, i.e. $h = \frac{1}{n}$. We show

	Robin					Wave guide					Dirichlet				
ϵ	1e-2	1e-3	1e-4	1e-5	1e-6	1e-2	1e-3	1e-4	1e-5	1e-6	1e-2	1e-3	1e-4	1e-5	1e-6
k	Schur complement block with $m = \frac{n}{2} - 1$														
20.1	5	6	7	7	8	6	6	7	7	8	4 (3)	5 (4)	6 (5)	6 (5)	7 (6)
40.2	8	10	10	11	12	9	10	10	11	11	7 (4)	9 (5)	10 (6)	10 (6)	11 (7)
80.4	12	14	16	18	18	14	15	17	18	18	11 (4)	14 (5)	15 (6)	17 (7)	18 (8)
160.8	18	22	24	28	30	23	26	27	29	30	19 (4)	23 (6)	25 (7)	27 (8)	29 (9)
321.6	29	34	40	44	47	38	41	44	46	49	30 (4)	36 (6)	41 (7)	43 (9)	46 (10)
643.2	50	59	67	73	79	67	72	76	80	83	46 (4)	61 (6)	68 (8)	72 (9)	76 (11)
k	Schur complement block with $m = \frac{n}{4} - 1$														
20.1	3	4	4	5	5	3	4	4	4	5	3 (2)	3 (3)	3 (3)	5 (3)	5 (4)
40.2	5	5	6	6	7	5	6	6	7	7	4 (2)	5 (3)	6 (3)	6 (3)	7 (4)
80.4	6	8	9	9	10	8	9	10	10	10	7 (2)	8 (3)	8 (3)	10 (3)	10 (4)
160.8	9	12	14	16	17	13	15	16	16	17	11 (2)	14 (3)	16 (3)	16 (4)	17 (4)
321.6	15	18	22	24	27	22	24	28	28	29	21 (2)	23 (3)	25 (3)	28 (4)	29 (4)
643.2	25	32	38	42	45	42	45	48	49	51	36 (2)	43 (3)	45 (3)	49 (4)	49 (4)
k	Schur complement block with $m = \frac{n}{8} - 1$														
20.1	3	3	3	3	3	3	3	3	3	3	3 (2)	3 (2)	3 (2)	3 (3)	3 (3)
40.2	3	4	4	4	5	3	4	4	4	5	3 (2)	4 (2)	4 (3)	4 (3)	5 (3)
80.4	4	5	6	6	7	5	5	6	6	7	5 (2)	5 (2)	6 (3)	6 (3)	6 (3)
160.8	6	8	9	9	10	8	9	9	10	10	8 (2)	8 (2)	9 (3)	10 (3)	10 (3)
321.6	9	11	13	15	16	14	15	16	16	17	13 (2)	15 (2)	15 (3)	16 (3)	17 (3)
643.2	12	17	22	24	27	22	26	27	29	30	22 (2)	26 (2)	28 (3)	29 (3)	29 (3)

Table 1. ϵ-rank in 2d for a matrix subblock $S_{m,k}$ with increasing k and three choices of m for 10 ppw (in parentheses for the Dirichlet case also the corresponding results for the Laplace operator are shown).

three cases: $m = \frac{n}{2} - 1$, which means a large block of the Schur complement, about a quarter of the entire matrix, just avoiding the diagonal, $m = \frac{n}{4} - 1$ which is about half the size and now away from the diagonal, and finally $m = \frac{n}{8} - 1$, which is a relatively small block, again halved once more, and very far from the diagonal. We clearly see that the ϵ-rank is growing, and the growth is similar in the case of Robin conditions, the wave guide case where we have Robin conditions on the left and right and Dirichlet conditions at the top and bottom, and the case with Dirichlet conditions all around. For comparison purposes, we also added the ϵ-rank for the Laplacian in parentheses in the Dirichlet case. Clearly the ϵ-rank is growing for increasing wave number k, whereas it is constant for the Laplace case as soon as the block is away from the diagonal, as expected from theory [7]. Figure 2 shows the results of Table 1 graphically, and we see that the ϵ-rank is growing algebraically in k, approximately like $O(k^{\frac{3}{4}})$ when the wave number k is increasing. This seems to be independent of the choice of the block determined by the parameter m, only the constant in front of the growth is getting smaller as the block size is getting smaller and is moved further away from the diagonal. Note however that comparing in Table 1 for example the fourth line for $m = \frac{n}{2} - 1$ with the fifth line for $m = \frac{n}{4} - 1$ and sixth line for $m = \frac{n}{8} - 1$, the ranks are not growing, which indicates that with a corresponding admissibility condition, k

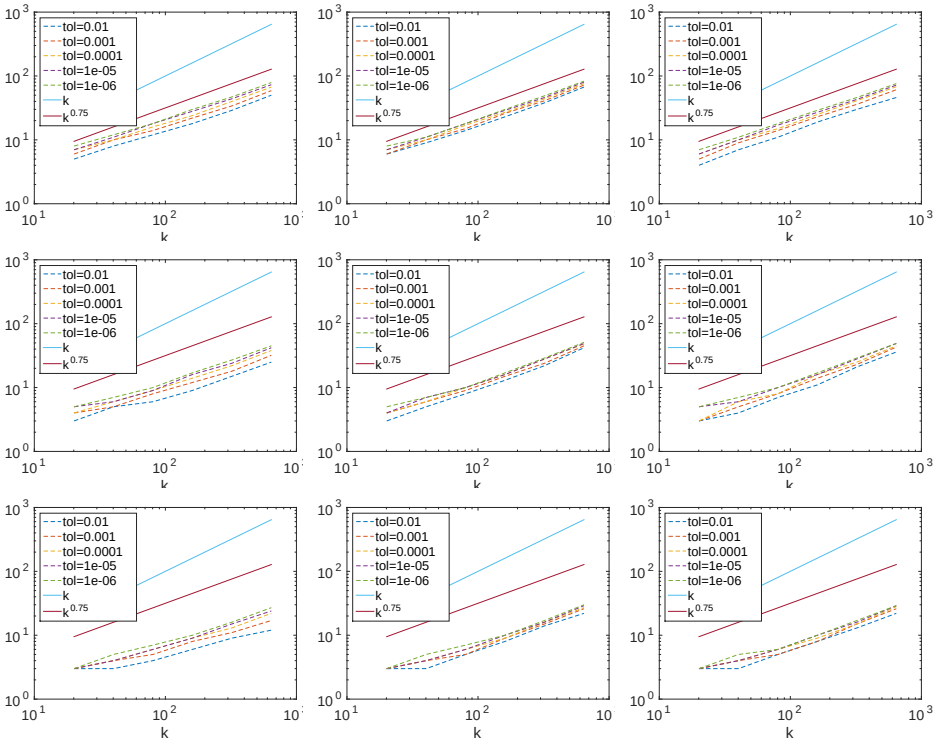

Fig. 2. Results of Table 1 shown graphically, together with two reference growth curves $O(k)$ and $O(k^{\frac{3}{4}})$.

independent compression will be possible. There will however be so many blocks then that $\mathcal{H}^2$-matrix techniques will be needed for almost linear complexity [6].

We now repeat the same experiment for the largest subblock under the condition that $k^3h^2 =$const, which is suggested to control the pollution effect [1]. We use the same grids as in Table 1, but for a more slowly increasing wave number k. We start with the same resolution as in Table 1 for $k = 20.1$, so the first lines indicating the ϵ-rank are the same in the top row for the largest subblock in Table 1 and the new Table 2. We see again that the ϵ-rank is growing as in the 10 ppw case, and it seems the growth rate is very similar to the case in Table 1 for corresponding wave numbers k. This indicates that it is not the mesh size, but really the wave number k that dictates the growth of the ϵ-rank.

We finally test Schur complements which are not just based on the variables on one side of the domain, but include more sides. The corresponding results are shown in Table 3. We see that when a neighboring side is included in the Schur complement, the ϵ-rank is growing already a bit faster, and when opposite sides or more are included, the growth becomes $O(k)$, see also [10] for a theoretical study of the influence of geometry.

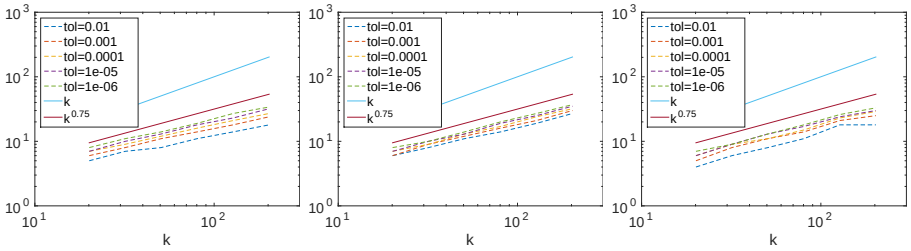

	Robin					Wave guide					Dirichlet				
ϵ	1e-2	1e-3	1e-4	1e-5	1e-6	1e-2	1e-3	1e-4	1e-5	1e-6	1e-2	1e-3	1e-4	1e-5	1e-6
k	Schur complement block with $m = \frac{n}{2} - 1$														
20.10	5	6	7	7	8	6	6	7	7	8	4	5	6	6	7
31.92	7	8	9	10	11	8	9	9	10	10	6	8	9	9	9
50.66	8	11	12	13	14	11	12	13	13	14	8	11	11	13	13
80.42	11	14	16	18	19	14	16	17	19	20	11	14	15	17	18
127.67	14	18	21	23	27	19	21	24	25	27	18	21	23	24	26
202.66	18	24	27	32	34	27	30	32	35	37	18	25	29	30	33

Table 2. ϵ-rank in 2d for the largest matrix subblock $S_{m,k}$ with $m = \frac{n}{2} - 1$ for increasing k for the same mesh refinement as in Table 1, but wave numbers k such that k^3h^2 =const (the Laplace case would be identical to Table 1).

3 Three Dimensional Study

We study now the three dimensional case of the Helmholtz equation as it appears in geophysical applications, namely

$$\Delta u + \frac{(2\pi\nu)^2}{V(x,y,z)^2} u = \delta(\overline{r} - \overline{r}_s) f \qquad \text{in } \Omega := (0, L)^3. \tag{5}$$

Here ν represents the frequency in Hz, $V(x, y, z)$ is a given velocity field with the velocity measured in $\frac{m}{s}$, $\overline{r}_s$ are the coordinates of a point source, whose strength is given by f, and L represents the size of the domain. We will test Dirichlet boundary conditions and perfectly matched layers (PMLs), for which we use an adaptation of the complex coordinate stretching elastic PML from [9]. We discretize the equation on a rectangular grid, and enumerate the nodes by going along the x-direction first, followed by the y-direction, and finally the z-direction. With this enumeration, the matrix subblock A_1 in (3) corresponds to the first x-y plane of discretization points, with associated Schur complement matrix S defined as in (4). We use the standard 7-point finite difference stencil, and an optimized 27-point finite difference stencil which reduces pollution and permits a reduction from 15 down to 4 ppw for equivalent results [28].

We start with a constant velocity $V(x, y, z) = 2400m/s$ in the cube domain with physical dimension $L = 1200m$. We simulate for the frequencies $\nu = 4Hz, 8Hz, 16Hz$ using the corresponding number of grid points $n = 20, 40, 80$, which implies that we are using 10 ppw in these experiments. We first show in Figure 3 a comparison on how the singular values decay for a large off diagonal

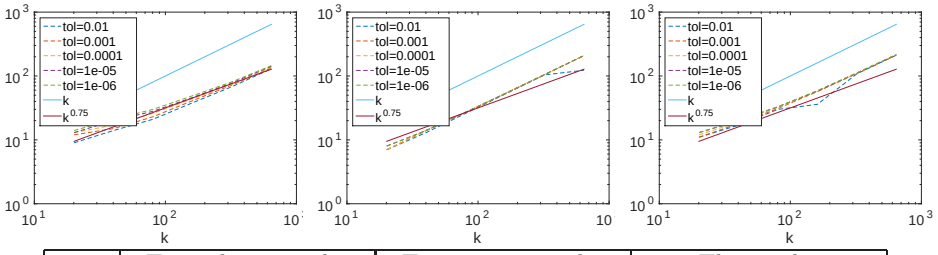

	Two adjacent sides					Two opposite sides					Three sides				
ϵ	1e-2	1e-3	1e-4	1e-5	1e-6	1e-2	1e-3	1e-4	1e-5	1e-6	1e-2	1e-3	1e-4	1e-5	1e-6
k	Schur complement block with $m = \frac{n}{2} - 1$														
20.10	9	12	13	13	14	7	7	7	8	8	11	11	12	13	13
31.92	14	15	17	20	21	13	14	14	14	14	17	18	19	20	20
50.66	21	23	26	28	30	26	27	27	27	27	30	31	32	33	33
80.42	38	41	44	46	49	52	53	53	53	53	36	57	58	58	59
127.67	68	72	74	78	81	104	105	105	105	105	108	109	110	111	112
202.66	130	134	138	142	145	123	208	209	209	209	212	213	214	215	217

Table 3. ϵ-rank in 2d for the largest matrix subblock $S_{m,k}$ with $m = \frac{n}{2} - 1$ in the Dirichlet case where the matrix subblock corresponds now to two adjacent, two opposite, and three sides of the domain, for increasing k for the same mesh refinement as in Table 1.

block, depending on the discretization stencil and the boundary condition. We clearly observe that increasing the frequency ν delays the decay of the singular values, and this does neither depend much on the discretization stencil, nor on the boundary condition.

We next present the ϵ-ranks of $S_{m,k}$ in Table 4, comparing the 7 point stencil to the 27 point stencil, and Dirichlet boundary conditions with PML boundary conditions using $n_{PML} = 5$ points in the PML layer. We see that the ϵ-rank grows when k increases, and the graphic visualization in Figure 4 shows that the growth is again algebraic, this time approximately $O(k^{\frac{4}{3}})$ for k large.

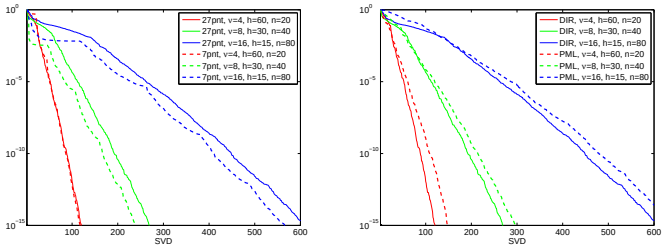

Fig. 3. Decay of the singular values in 3d, comparing the 27 and 7 point stencil with Dirichlet conditions (left) and Dirichlet and PML boundary conditions for the 27 point stencil (right) for a large matrix subblock $S_{m,k}$ corresponding to the top row in Table 4.

			7-point, Dirichlet					27-point, Dirichlet					27-point, PML				
		ϵ	1e-2	1e-3	1e-4	1e-5	1e-6	1e-2	1e-3	1e-4	1e-5	1e-6	1e-2	1e-3	1e-4	1e-5	1e-6
n	ν	k	Schur complement block with $m = \frac{(n-1)^2-1}{2}$														
20	4	0.0052	27	37	46	51	59	27	35	43	53	59	29	39	49	61	71
40	8	0.0105	6	54	68	85	110	61	78	94	112	129	58	76	97	120	140
80	16	0.0209	32	147	180	230	276	145	185	224	263	306	141	189	237	287	325
n	ν	k	Schur complement block with $m = \frac{(n-1)^2-1}{4}$														
20	4	0.0052	5	7	9	11	15	5	7	9	11	14	8	15	20	25	32
40	8	0.0105	6	13	17	21	23	16	19	23	25	27	11	16	23	29	35
80	16	0.0209	25	46	60	67	72	41	59	67	76	79	36	48	63	74	81
n	ν	k	Schur complement block with $m = \frac{(n-1)^2-1}{8}$														
20	4	0.0052	4	6	6	8	10	4	6	6	8	10	7	12	15	18	21
40	8	0.0105	5	9	9	15	17	9	13	16	18	21	8	13	15	21	24
80	16	0.0209	17	31	38	44	52	31	38	42	51	52	23	35	40	48	53

Table 4. ϵ-rank in 3d for a matrix subblock $S_{m,k}$ with increasing k and three choices of m.

		n=40, $\nu = 8$, subblock 760×760							n=80, $\nu = 16$, subblock 3120×3120						
n_{PML}	ϵ	1e-2	1e-3	1e-4	1e-5	1e-6	L_1	L_∞	1e-2	1e-3	1e-4	1e-5	1e-6	L_1	L_∞
0		61	78	94	112	129	1.00	1.00	145	185	224	263	306	1.00	1.00
2		57	78	96	123	140	0.12	0.10	148	197	245	291	330	0.56	0.18
4		58	77	97	120	140	0.046	0.043	144	194	242	290	327	0.34	0.10
8		58	78	99	121	142	0.036	0.039	130	181	230	273	322	0.10	0.044
16		59	80	103	125	145	0.036	0.039	117	162	215	265	306	0.036	0.039

Table 5. Solution error and ϵ-rank in 3d for the largest subblock with different PML depth.

To test the impact of the quality of the PML on the ϵ-rank, we show in Table 5 the ϵ-rank for an increasing depth a of the PML, for $V(x, y, z) = 2400m/s$ on the cube $1200m \times 1200m \times 1200m$ as before, for two meshes with 40 and 80 grid points in each direction and frequency $\nu = 8$ and $\nu = 16$, so we have 10 ppw. We see that improving the PML does not reduce the ϵ-rank. We also show in Table 5 the relative error in the L_1 and L_∞ norms comparing with a closed form solution, which indicates that for $n = 40$, we reach the truncation error of the discretization at $n_{PML} = 8$, since increasing the PML depth does not reduce the error further.

We next study the behavior of the ϵ-rank in a random medium $V(x, y, z)$ using the same geometry as before. We show in Figure 5 the decay of the singular values comparing the constant to the random medium case when using a fixed number of ppw. We see that the decay of the singular values in the random medium case is comparable to the decay of the singular values in the constant medium case, just the small ones decay a bit more slowly. This is further illustrated for the ϵ-rank in Table 6, which corresponds to Table 4 just with random velocity, and the results are similar.

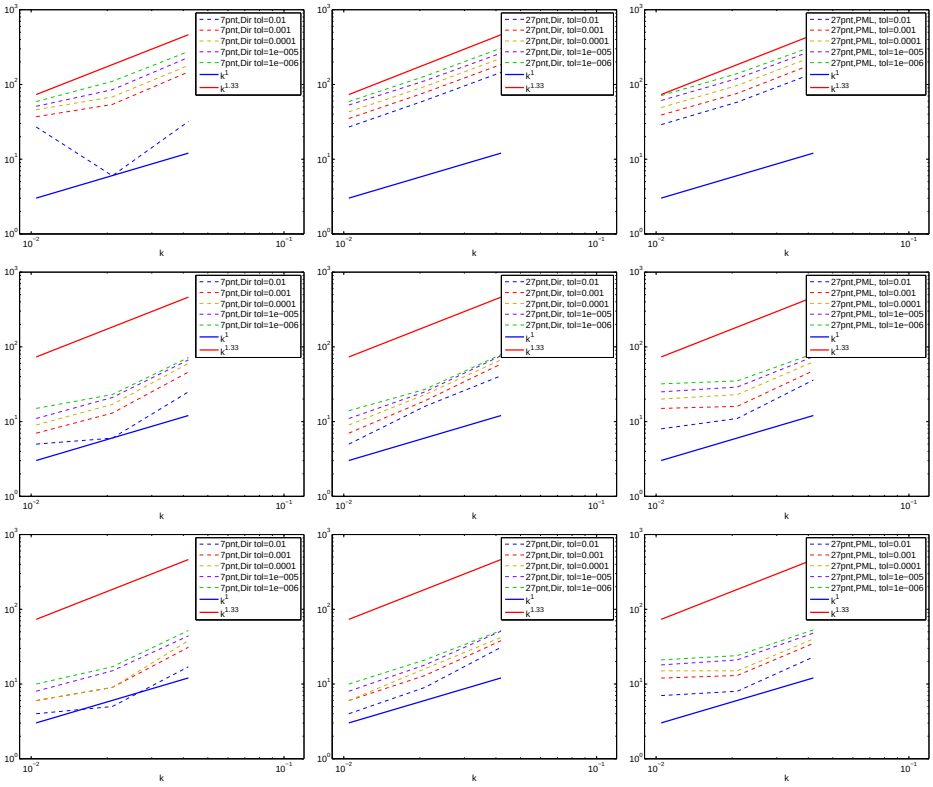

Fig. 4. Results of Table 4 shown graphically, together with two reference growth curves $O(k)$ and $O(k^{\frac{4}{3}})$.

We finally test Schur complement blocks which are not just based on the variables on one side of the domain, but include more sides. We use in this experiment as the domain just the unit cube, $L = 1$, the constant velocity field $V(x, y, z) = 1$, and Dirichlet boundary conditions. The corresponding results shown in Table 7 indicate that as soon as the Schur complement includes opposite sides, the ϵ-rank is growing quadratically in the wave number.

4 Conclusion

We studied numerically the compressibility of subblocks of Schur complement matrices stemming from discretized Helmholtz problems. We experimentally found that the ϵ-rank is growing algebraically in the wave number k if the block size is chosen in a fixed proportion of the Schur complement matrix, which corresponds to a fixed region in physical space of the corresponding Green's function. The growth does not depend on the boundary conditions of the underlying problem, but the choice of which variables are eliminated in forming the

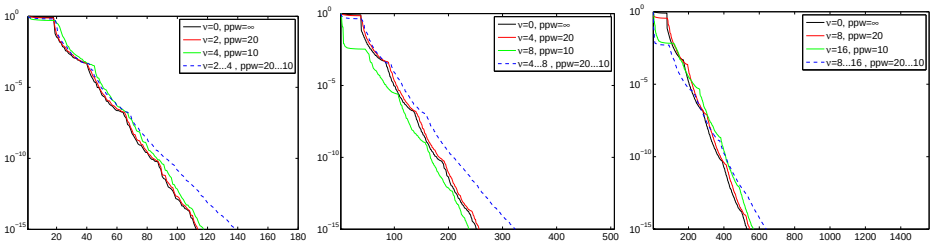

Fig. 5. Comparison of the decay of the singular values in 3d (7 point stencil with Dirichlet conditions) between a homogeneous medium and a random field varying from $2Hz$ to $4Hz$ with $n = 20$ number of grid points in each direction (left); $4Hz$ to $8Hz$, $n = 40$ (middle) and $8Hz$ to $16Hz$, $n = 80$ (right)

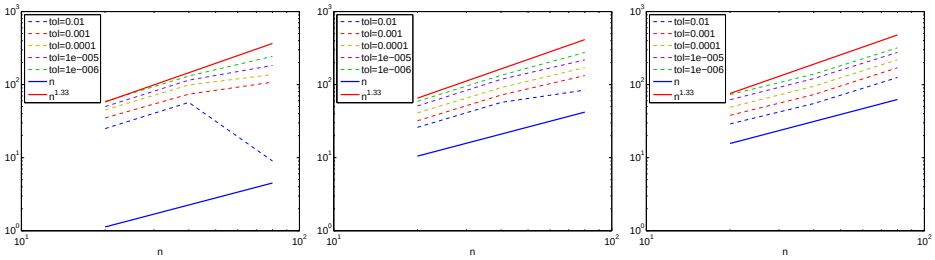

		7-point, Dirichlet					27-point, Dirichlet					27-point, PML				
	ϵ	1e-2	1e-3	1e-4	1e-5	1e-6	1e-2	1e-3	1e-4	1e-5	1e-6	1e-2	1e-3	1e-4	1e-5	1e-6
n	ν	Schur complement block with $m = \frac{(n-1)^2-1}{2}$														
20	2-4	25	35	45	50	59	26	32	41	51	59	29	38	49	62	73
40	4-8	57	74	99	115	131	57	72	91	118	134	55	73	95	121	139
80	8-16	9	108	137	183	244	84	133	171	218	275	125	170	219	276	319

Table 6. ϵ-rank in 3d for a large matrix subblock $S_{m,k}$ for a random velocity field with increasing n.

Schur complement. If opposite sides of the domain are kept, the worst growth is observed, namely $O(k)$ in 2d and $O(k^2)$ in 3d.

Acknowledgments: The research described was partially supported by RFBR grants 16-05-00800,17-01-00399 and the Russian Academy of Sciences Program "Arctic".

References

1. I. M. Babuska and S. A. Sauter. Is the pollution effect of the FEM avoidable for the Helmholtz equation considering high wave numbers? *SIAM J. Num. Anal.*, 34(6):2392–2423, 1997.
2. L. Banjai and W. Hackbusch. Hierarchical matrix techniques for low- and high-frequency Helmholtz problems. *IMA J. Numer. Anal.*, 28:46–79, 2008.
3. M. Bebendorf. *Hierarchical Matrices: A Means to Efficiently Solve Elliptic Boundary Value Problems.* Springer, 2008.

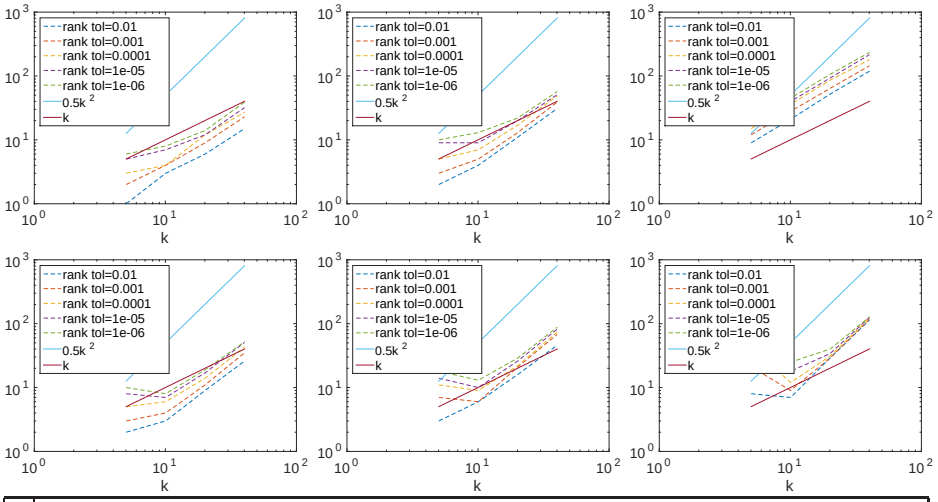

	Schur complement for one side														
ϵ	1e-2	1e-3	1e-4	1e-5	1e-6	1e-2	1e-3	1e-4	1e-5	1e-6	1e-2	1e-3	1e-4	1e-5	1e-6
k	Small block $m = \frac{(n-1)^2-1}{8}$					Medium block $m = \frac{(n-1)^2-1}{4}$					Large block $m = \frac{(n-1)^2-1}{2}$				
5	1	2	3	5	6	2	3	5	9	10	9	12	15	17	19
10	3	4	4	7	8	4	5	7	9	13	21	28	36	40	45
20	6	9	12	12	14	11	13	17	20	22	52	64	86	93	106
40	15	23	27	32	39	31	39	49	51	57	119	145	180	216	234
	Schur complement for two opposite sides														
k	Small block $m = \frac{(n-1)^2-1}{4}$					Medium block $m = \frac{(n-1)^2-1}{2}$					Large block $m = (n-1)^2-1$				
5	2	3	5	8	10	3	7	11	14	18	8	21	43	48	48
10	3	4	6	7	8	6	6	9	10	13	7	9	12	18	25
20	9	11	14	17	19	16	21	22	26	29	29	29	31	34	40
40	26	35	43	51	52	46	68	74	82	88	114	118	122	126	128

Table 7. ϵ-rank in 3d for a small, medium and large matrix subblock $S_{m,k}$ of a Schur complement for one side, and two opposite sides of the unit cube, for increasing k keeping 10 ppw.

4. M. Bebendorf and W. Hackbusch. Existence of $\mathcal{H}$-matrix approximants to the inverse FE-matrix of elliptic operators with L^∞-coefficients. *Num. Math.*, 95(1):1–28, 2003.
5. T. Betcke, E. van 't Wout, and P. Gélat. Computationally efficient boundary element methods for high-frequency Helmholtz problems in unbounded domains. *preprint*, 2016.
6. S. Börm and J. M. Melenk. Approximation of the high-frequency Helmholtz kernel by nested directional interpolation. *arXiv preprint arXiv:1510.07189*, 2015.
7. S. Chandrasekaran, P. Dewilde, M. Gu, and N. Somasunderam. On the numerical rank of the off-diagonal blocks of Schur complements of discretized elliptic PDEs. *SIAM J. Matrix Anal. Appl.*, 31(5):2261–2290, 2010.
8. R. Coifman, V. Rokhlin, and S. Wandzura. The fast multipole method for the wave equation: a pedestrian prescription. *IEEE Antennas and Propagation Magazine*,

35(3):7–12, 1993.
9. F. Collino and C. Tsogka. Application of the perfectly matched layer absorbing layer model to the linear elastodynamic problem in anisotropic heterogeneous media. *Geophysics*, 66:294–307, 2001.
10. K. Delamotte. *Une étude du rang du noyau de l'équation de Helmholtz: application des $\mathcal{H}$-matrices à l'EFIE*. PhD thesis, University Paris 13, 2016.
11. B. Engquist and L. Ying. Sweeping preconditioner for the Helmholtz equation: hierarchical matrix representation. *Comm. Pure Appl. Math.*, 64(5):697–735, 2011.
12. B. Engquist and L. Ying. Sweeping preconditioner for the Helmholtz equation: moving perfectly matched layers. *Multiscale Modeling & Simulation*, 9(2):686–710, 2011.
13. B. Engquist and H. Zhao. Approximate separability of Green's function for high frequency Helmholtz equations. Technical report, DTIC Document, 2014.
14. O. G. Ernst and M. J. Gander. Why it is difficult to solve Helmholtz problems with classical iterative methods. In *Numerical analysis of multiscale problems*, pages 325–363. Springer, 2012.
15. M. J. Gander. Optimized Schwarz methods. *SIAM J. Numer. Anal.*, 44(2):699–731, 2006.
16. M. J. Gander, L. Halpern, and F. Magoules. An optimized Schwarz method with two-sided Robin transmission conditions for the Helmholtz equation. *Int. J. Numer. Meth. Fluids*, 55(2):163–175, 2007.
17. M. J. Gander, F. Magoules, and F. Nataf. Optimized Schwarz methods without overlap for the Helmholtz equation. *SIAM J. Sci. Comput.*, 24(1):38–60, 2002.
18. M. J. Gander and F. Nataf. AILU for Helmholtz problems: a new preconditioner based on the analytic parabolic factorization. *J. Comput. Acoust.*, 9(04):1499–1506, 2001.
19. M. J. Gander and F. Nataf. An incomplete LU preconditioner for problems in acoustics. *J. Comput. Acoust.*, 13(03):455–476, 2005.
20. M. J. Gander and H. Zhang. Iterative solvers for the Helmholtz equation: Factorizations, sweeping preconditioners, source transfer, single layer potentials, polarized traces, and optimized Schwarz methods. *submitted*, 2016.
21. L. Greengard, D. Gueyffier, P.-G. Martinsson, and V. Rokhlin. Fast direct solvers for integral equations in complex three-dimensional domains. *Acta Numerica*, 18:243–275, 2009.
22. L. Greengard and V. Rokhlin. A fast algorithm for particle simulations. *J. Comput. Phys.*, 73(2):325–348, 1987.
23. W. Hackbusch. A sparse matrix arithmetic based on $\mathcal{H}$-matrices. part i: Introduction to $\mathcal{H}$-matrices. *Computing*, 62(2):89–108, 1999.
24. W. Hackbusch. *Hierarchical matrices: Algorithms and analysis*, volume 49. Springer, 2015.
25. B. Lizé. *Résolution directe rapide pour les éléments finis de frontière en électromagnétisme et acoustique: -Matrices. Parallélisme et applications industrielles*. PhD thesis, Université Paris-Nord-Paris XIII, 2014.
26. P. G. Martinsson and V. Rokhlin. A fast direct solver for scattering problems involving elongated structures. *J. Comput. Phys*, 221:288–302, 2007.
27. V. Rokhlin. Rapid solution of integral equations of scattering theory in two dimensions. *J. Comput. Phys.*, 86(2):414–439, 1990.
28. S. Solovyev and D. Vishnevsky. A dispersion minimizing finite difference scheme and multifrontal hierarchical solver for the 3d Helmholtz equation. In *The 12th International Conference on Mathematical and Numerical Aspects of Wave Propagation July 20-24 (WAVES 2015)*, pages 428–429, 2015.